Crack initiation characteristics and fatigue property of a high-strength steel in VHCF regime under different stress ratios

Xiaolong Liu, Chengqi Sun, Youshi Hong
State Key Laboratory of Nonlinear Mechanics, Institute of Mechanics, Chinese Academy of Sciences, Beijing 100190, China
hongys@imech.ac.cn

ABSTRACT. Crack initiation characteristics and fatigue property of a high-strength steel in very-high-cycle fatigue (VHCF) regime under different stress ratios were investigated in this paper. Fatigue tests were performed at stress ratios of -1, -0.5, 0.1 and 0.3 by using an ultrasonic fatigue testing machine. The difference of S-N data and the characteristics of crack initiation under different stress ratios were examined. It is shown that the magnitude of stress ratio has a substantial effect on the fatigue strength that decreases with the increase of stress ratio. However, the variation tendency of the S-N data from low-cycle fatigue to VHCF regime is similar for the four cases. SEM observations of the fracture surface indicate that fatigue crack initiates from the surface of specimen in low-cycle regime and initiates mostly from the inclusion in the interior of specimen in high-cycle and VHCF regimes, which is irrespective of the state of stress ratio. By means of Focused Ion Beam technique, the samples of crack initiation region were prepared then observed via TEM. The observations show the microscopic morphology of the crack initiation region, showing the different crack initiation characteristics and revealing the mechanism of crack initiation for different stress ratios. Moreover, the effect of inclusion size on fatigue life is discussed with the results showing that the effect of stress ratio and inclusion size on fatigue strength is well described by our proposed formula.

KEYWORDS. High-strength steel; Very-high-cycle fatigue; Crack initiation characteristics; Stress ratio; Inclusion size.

INTRODUCTION

In recent years, the research of very-high-cycle fatigue (VHCF) property has attracted increased interests because more and more engineering structures are required to endure 10^7 or even more fatigue cycles, and engineering alloys such as high-strength steels and titanium alloys exhibit a sharp decrease in fatigue strength between fatigue life of 10^6 and 10^9 cycles [1, 2]. Naito et al [3, 4] first reported that high-strength steels failed at the stress lower than the conventional fatigue limit and the crack initiated from non-metallic inclusions at the interior of specimen. The whole region of crack initiation and early propagation exhibits a "fish-eye" pattern and a relatively rough granular morphology is often observed surrounding the inclusion, which is called fine granular area (FGA) [5-7]. Several models have been proposed for explaining the formation mechanism of FGA, including "formation and debonding of fine granular layer"

[8], "hydrogen assisted crack growth" [9], and "decohesion of spherical carbide" [10]. However, the formation mechanism of FGA is still not clearly understood, and needs more investigation.

Fatigue tests are time-consuming and expensive especially for the fatigue of large number of cycles. The application of ultrasonic fatigue machine (frequency about 20 kHz) greatly cuts the testing time for VHCF of metallic materials and has accumulated a large amount of VHCF data [11, 12]. For example, Kovacs et al [13] investigated the effects of mean stress on fatigue life of a low-carbon steel by using ultrasonic fatigue machine. In their results, the continuous S-N curves presented the same tendency for all the stress ratios, but FGA was only observed at R=–1. Sander et al [14] also used ultrasonic frequency testing to investigate the effects of mean stress and variable stress on the fatigue property of a medium-carbon steel, and reported that FGA was not observed for all stress ratios. Shiozawa et al [15] (used frequency 80 Hz) and Sakai et al [16] (used frequency 50 Hz) investigated the effects of stress ratio on the VHCF property of a high-strength steel, SUJ2, by using conventional frequency fatigue machine, respectively. In their results, the FGA turned obscure with the increase of stress ratio.

The effects of stress ratio on the fatigue strength of metallic materials have been an important topic. For low-cycle and high-cycle fatigue, Goodman formula and Gerber formula are usually used to correlate stress ratio and fatigue strength. However, for VHCF regime, the application of these two formulae needs more validation. Murakami et al [17, 18] proposed a model for predicting the fatigue strength of high-strength steels, which combined the fatigue strength σ (MPa), stress ratio R, Vicker hardness Hv (kgf/mm^2) and the square root of inclusion or defect projection area as follows:

$$\sigma = \frac{C(\mathrm{Hv}+120)}{\left(\sqrt{area}\right)^{1/6}}\left(\frac{1-R}{2}\right)^{\alpha} \tag{1}$$

where α=0.226+Hv×10^4, C=1.43 for surface inclusions or defects and C=1.56 for interior inclusions or defects.

Recently, Sun et al [19, 20] developed a model for estimating the effects of stress ratio and inclusion size on fatigue strength for high-strength steels with fish-eye mode failure based on experimental results:

$$\sigma_{a,R} = CN^{l}a_0^{m}\left(\frac{1-R}{2}\right)^{\alpha} \tag{2}$$

where C, l and α are material parameters obtained by fitting the experimental data, and a_0 denotes the inclusion size. The model of Eq. (2) incorporates the effect of fatigue life on fatigue strength, and the model of Eq. (1) is a special case of Eq. (2).

In this paper, the effects of stress ratio on VHCF property of a high-strength steel, GCr15, were investigated. Fatigue test was performed by using ultrasonic (20 kHz) fatigue test machine with a value of mean stress superimposed. The stress ratios were -1, -0.5, 0.1 and 0.3. The microstructure below FGA for the fracture surfaces at R=-1 and R=0.3 was observed by transmission electron microscopy (TEM). The observations show the different crack initiation characteristics and reveal the mechanism of crack initiation for different stress ratios. Moreover, the effect of inclusion size on fatigue life is discussed with the results showing that the effect of stress ratio and inclusion size on fatigue strength is well described by our proposed formula.

MATERIALS AND TESTING METHODS

Materials

The material used in this investigation is a high-carbon chromium bearing steel (GCr15). The main chemical compositions (mass percentage) are: 1.04 C, 1.51 Cr, 0.29 Mn, 0.24 Si, 0.0058 P, 0.0030 S and balance Fe. Specimens were machined into hourglass shape from annealed steel bar. Then, the specimens were heated at 845°C for 1 hour in vacuum, oil-quenched and tempered for 2 hours in vacuum at 180 ℃, and air-cooling. Fig. 1 presents the microstructure of the heat-treated material, which is typical martensite structure with spherical carbide particles distributed randomly in the matrix.

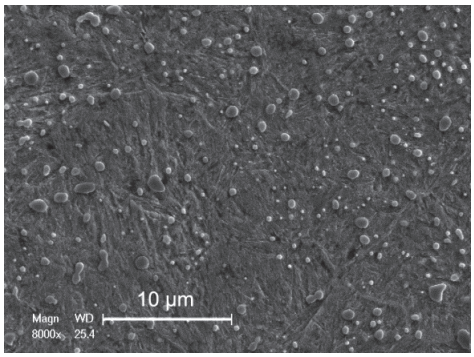

Figure 1: Microstructure photo of tested material by SEM.

Testing methods

An MTS 810 system was used to conduct the tensile test with cylindrical specimens of 6 mm in diameter at a strain rate of 10^{-4} s^{-1}. Five tensile specimens were tested, and the average value of the tensile strength was 1896 MPa. The micro-hardness measurement was performed on three samples by a micro-hardness tester at a load of 50 g with the load holding time of 15 s. Twenty points were tested in each sample, and the average value of micro-hardness was 760 kgf/mm^2.
Fatigue test was conducted by using an ultrasonic fatigue test machine at a resonance frequency of 20 kHz at room temperature, and air-cooling was used to cool the specimens during ultrasonic fatigue test. The ultrasonic fatigue machine was hung in a tensile machine. The amplitude stress was loaded by the ultrasonic fatigue machine, and the mean stress was superimposed by the tensile machine. Stress ratios of -1, -0.5, 0.1 and 0.3 were chosen. The geometries of the specimens are shown in Fig. 2. Before fatigue test, the round notch surface of each specimen was ground and polished to eliminate machine scratches. The fracture surfaces of the failed specimens were observed by using a field-emission type scanning electron microscope (SEM). Moreover, Focused Ion Beam (FIB) technique was used to prepare the Transmission Electron Microscopy (TEM) samples of crack initiation region. Then, the samples were observed via TEM.

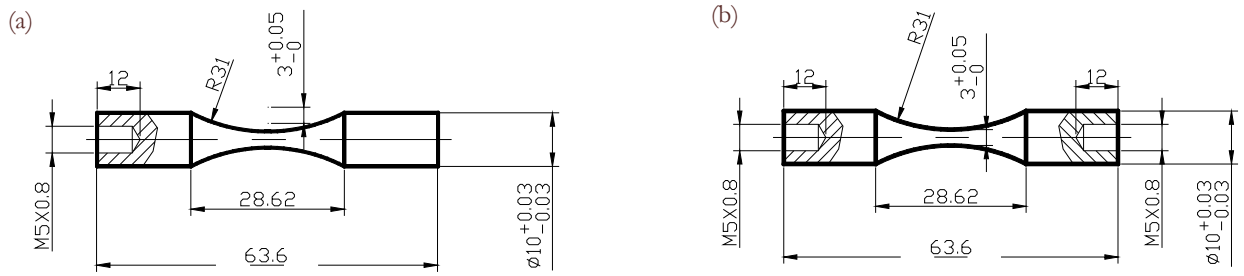

Figure 2: Shape and dimension (in mm) of specimens. (a) For testing without mean stress (R=–1), and (b) For testing with superimposed mean stress (R≠–1).

EXPERIMENTAL RESULTS AND ANALYSES

S-N curves

Fig. 3 presents the *S-N* curves for the tests at the four stress ratios. It is seen from Fig. 3 that the tendency of the S-N curves from low-cycle fatigue to VHCF is similar for all the four stress ratios. But the stress ratio has a substantial effect on the fatigue strength, which decreases with the increase of stress ratio.

Characterization of crack initiation region

Fig. 4 presents the typical morphology of the fracture surfaces for the specimens at the stress ratio of –1. As shown in Fig. 4, the fracture surface of specimens is divided into the following four types. Type I: Crack initiated from surface without

inclusion observed at initiation region [Fig. 4(a)]. Type II: Crack initiated from surface with surface or subsurface inclusion at initiation region [Fig. 4(b)]. Type III: Crack initiated from interior with inclusion and without FGA at initiation region [Fig. 4(c)]. Type IV: Crack initiated from interior with inclusion and FGA at initiation region [Fig. 4(d)]. The fatigue process associated with Type I and Type II is mainly in low-cycle fatigue regime, the fatigue process associated with Type III is mainly in high-cycle fatigue regime, and the fatigue process associated with Type IV is in VHCF regime.

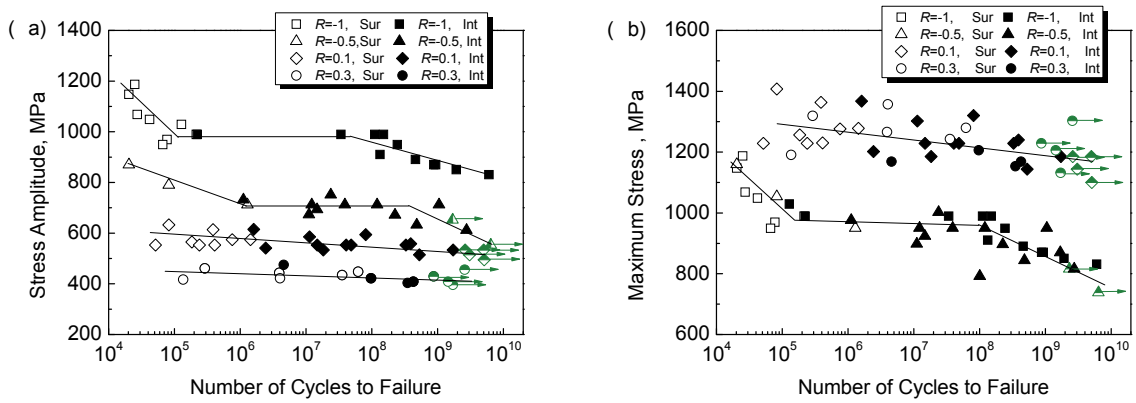

Figure 3: S-N curves of specimens with stress ratios of -1, -0.5, 0.1 and 0.3. (a) In terms of stress amplitude, and (b) In terms of the maximum stress (Sur: surface initiation, Int: interior initiation, Symbol with arrow: no broken.)

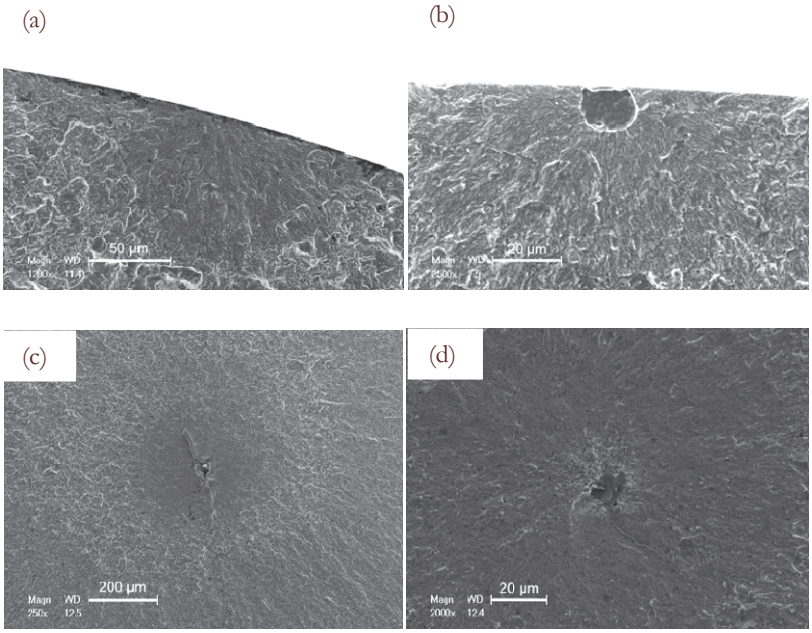

Figure 4: Typical examples of morphology of fracture surfaces for R=-1. (a) Crack initiated from surface without inclusion, σ_a= 1048 MPa, N_f=4.20×10^4 , (b) Crack initiated from surface with inclusion, σ_a=1147 MPa, N_f=2.03×10^4, (c) Crack initiated from interior inclusion without FGA, σ_a = 1029 MPa, N_f=1.28×10^5, and (d) Crack initiated from interior inclusion with FGA, σ_a= 989 MPa, N_f=1.11×10^8.

Fig. 5 presents the patterns of failed specimen with fatigue cracks initiated from inclusion with FGA morphology for the four stress ratios. It is seen from Fig. 5 that the morphology of FGA is very clear at the stress ratios of -1 and -0.5. However, for the stress ratios of 0.1 and 0.3, the morphology of FGA becomes obscure. In order to observe the microstructure below the FGA region, two fracture surfaces were chosen as shown in Fig. 5(a) and (d). The rectangle marks in Fig. 5(a) and (d) were the locations for the TEM samples cut by FIB, respectively. The samples were observed by TEM, and the diameter of electron diffraction area is 200 nm. The selected area diffraction (SAD) patterns of the sample from the crack initiation region at R=-1 in Fig. 6(b) and (c) show the discontinuous diffraction circles for the FGA region,

indicating that several grains exist within the diffraction area of 200 nm in diameter. This phenomenon verifies the existence of fine granular area. However, the SAD patterns of that at R=0.3 in Fig. 7(b) and (c) show the isolated spots, indicating only a single grain in the diffraction area. Both the SAD patterns of that away from the FGA in Fig. 6(d) and Fig. 7(d) are isolated spots, which is regardless of stress ratio. These results support our recent proposed mechanism of numerous cyclic pressing between crack surfaces for the formation of FGA [21].

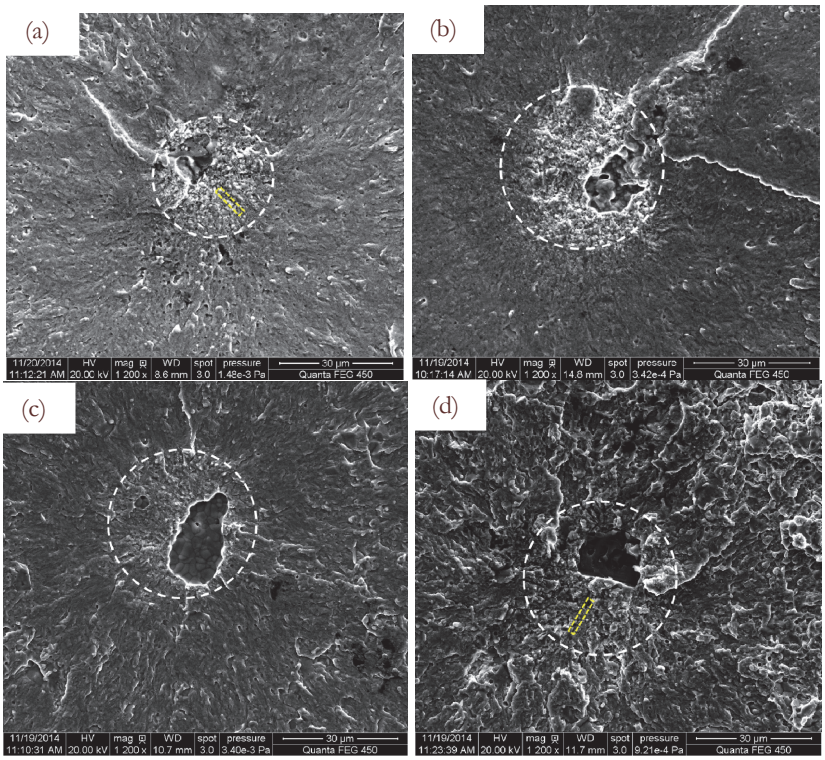

Figure 5: Typical examples of morphology of failed specimens with cracks initiated from interior inclusion with FGA (marked with dotted circle) for the four stress ratios. (a) R=-1, σ_a=989 MPa, N_f=1.11×10^8, (b) R=-0.5, σ_a=633 MPa, N_f=4.81×10^8, (c) R=0.1, σ_a=534 MPa, N_f=1.84×10^7, and (d) R=0.3, σ_a=430 MPa, N_f=8.70×10^8.

Effects of stress ratio and inclusion on the fatigue strength

The inclusion size $area_{inc}$ at the crack initiation site was measured from the SEM images of fracture surface, which is the projection area of inclusion. Fig. 8 presents the relation between the fatigue life and the inclusion size. It is seen from Fig. 8 that the size of the inclusion is scattered between 6 μm and 69 μm, and most of them is mainly distributed between 6 μm and 20 μm. The size of inclusion is independent of fatigue life and stress ratio.

Our previous research has shown that the fatigue strength involving the effect of stress ratio and inclusion size is expressed as [20]

$$\sigma_{a,R} = CN^{l} a_0^{m} \left(\frac{1-R}{2} \right)^{\alpha} \tag{3}$$

where C, l and m are material parameters, and a_0 denotes the inclusion size.

Here, Eq. (3) is used to correlate the effect of stress ratio and inclusion size on fatigue strength. The parameter m is taken as -1/6 [18]. The parameters C=e$^{10.5}$ and l=-0.0511 are determined by fitting experimental data of failed specimens with cracks initiated from specimen interior with FGA at R=–1, and the parameter α is calculated as 0.713 by taking C=e$^{10.5}$ and l=-0.0511 and using the experimental data of failed specimens with cracks initiated from specimen interior with FGA at R=0.1.

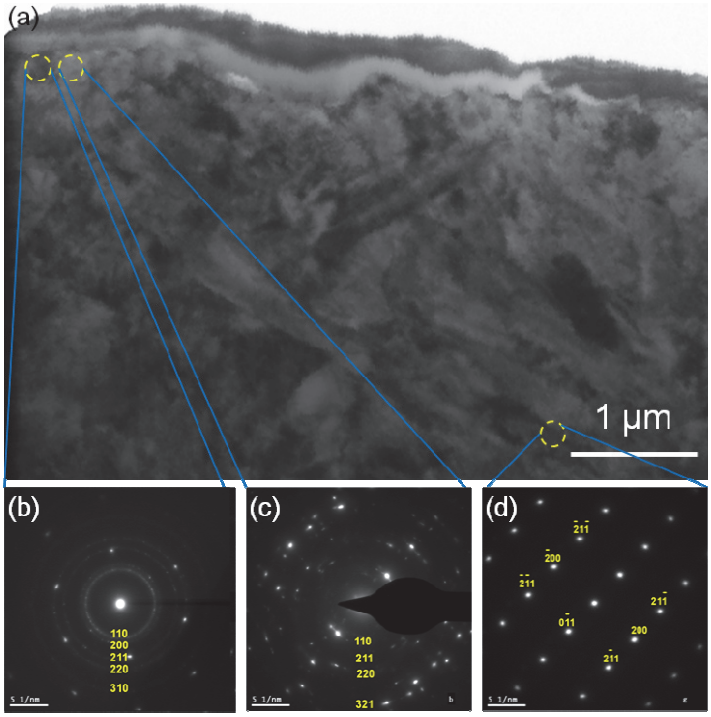

Figure 6: SAD patterns of TEM sample from crack initiation region of fracture surface at *R*=-1.

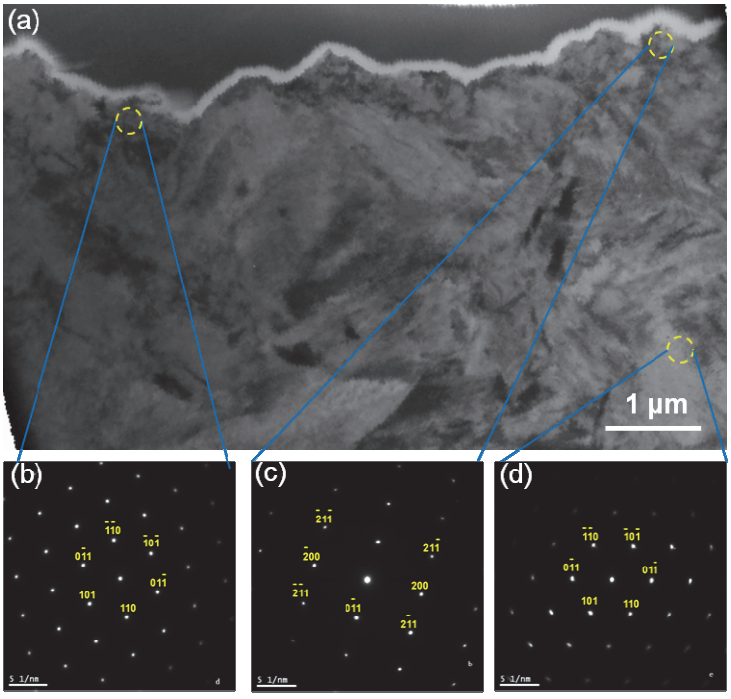

Figure 7: SAD patterns of TEM sample from crack initiation region of fracture surface at *R*=0.3.

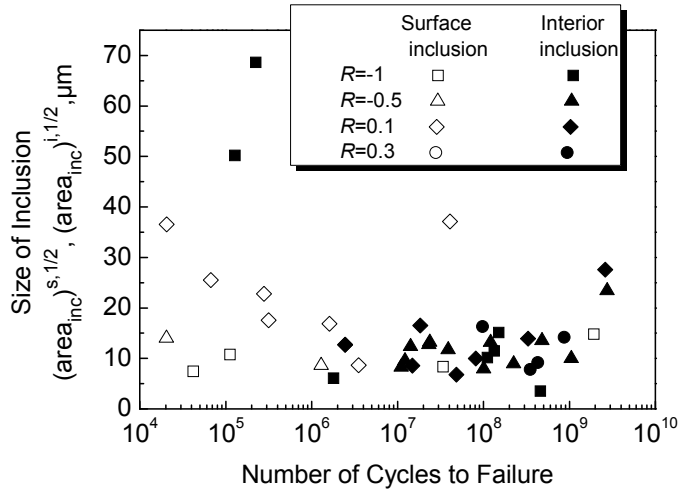

Figure 8: Relationship between inclusion size and fatigue life for four tested stress ratios.

Fig. 9 presents the comparison of the fatigue strength obtained by Eq. (3) using different inclusion sizes with the experimental data at different stress ratios. It is seen that the estimated fatigue strength by using the minimum inclusion size of the specimens is generally higher than the experimental results, which is regarded as the upper bound of the fatigue strength obtained by experiments. While the estimated fatigue strength using the maximum inclusion size is generally lower than the experimental ones, which is regarded as the lower bound of the fatigue strength obtained by experiments. The fatigue strength obtained by Eq. (3) using the average inclusion size is moderate, which seems to be the medium S–N curve. This indicates that Eq. (3) is suitable for the description of the effect of inclusion size and stress ratio on fatigue strength.

It is noted that the shape of S–N curve for high-strength steels often presents a duplex pattern corresponding to surface-initiated fracture mode and interior-initiated fracture mode. Here, we only consider the interior-initiated fracture mode with an FGA surrounding the inclusion at crack origin.

Comparison with Goodman formula and Gerber formula

Goodman formula and Gerber formula are classic models for the effect of mean stress on fatigue strength. Here, the present model is compared with Goodman formula and Gerber formula for predicting the effect of stress ratio on the fatigue strength in VHCF regime. The present model, Goodman formula and Gerber formula are written as follows.

Present model:

$$\sigma_{m,\mathrm{R}} = \sigma_{a,\mathrm{R}} \left[\left(\frac{\sigma_{-1}}{\sigma_{a,\mathrm{R}}} \right)^{\frac{1}{\alpha}} - 1 \right] \tag{4}$$

Goodman formula:

$$\sigma_{m,\mathrm{R}} = \sigma_{\mathrm{b}} \left(1 - \frac{\sigma_{a,\mathrm{R}}}{\sigma_{-1}} \right) \tag{5}$$

Gerber formula:

$$\sigma_{m,\mathrm{R}} = \sigma_{\mathrm{b}} \left(1 - \frac{\sigma_{a,\mathrm{R}}}{\sigma_{-1}} \right)^{\frac{1}{2}} \tag{6}$$

where $\sigma_{m,R}$ is mean stress with respect to R, $\sigma_{a,R}$ is stress amplitude with respect to R, σ_b is tensile strength, and σ_{-1} is stress amplitude at R=-1.

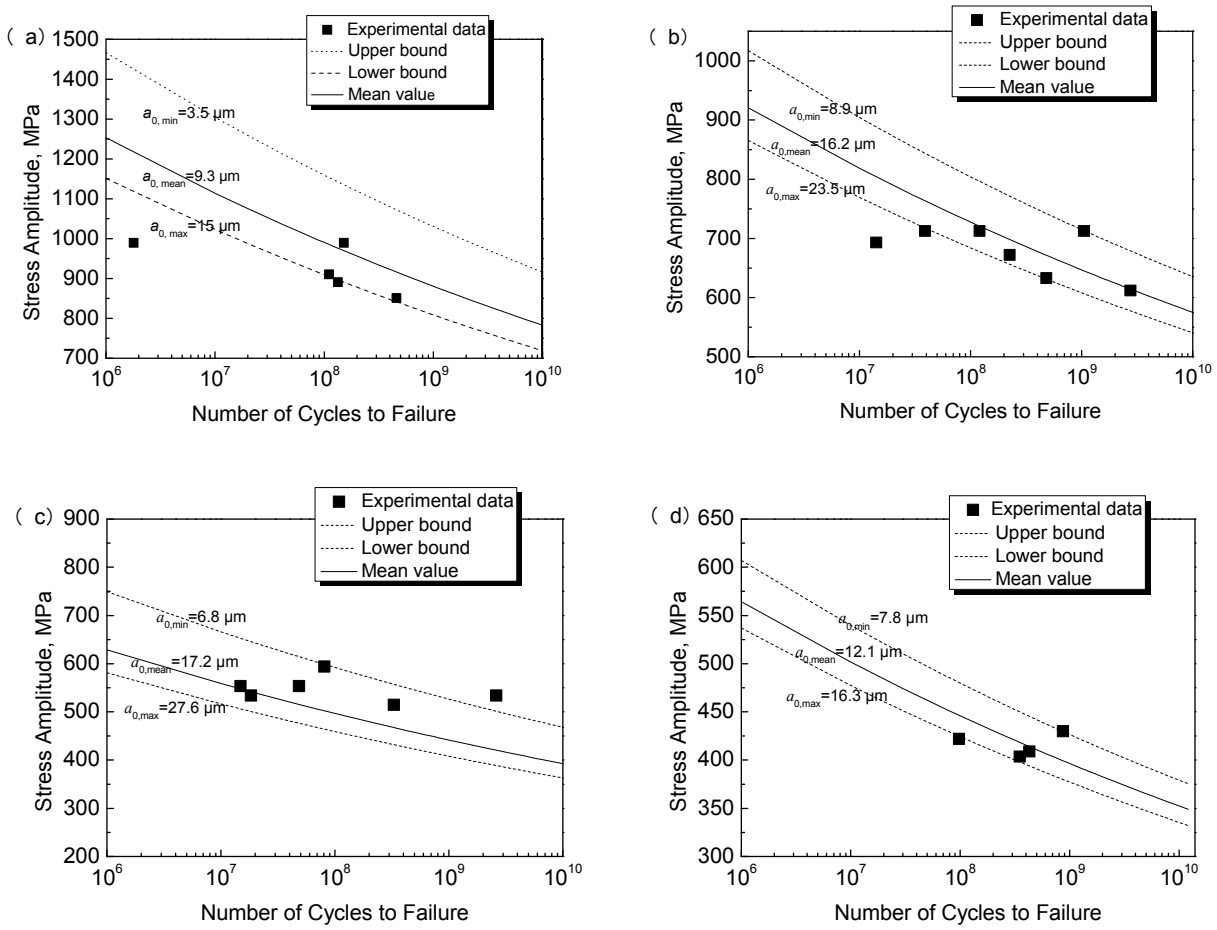

Figure 9: Comparison of fatigue strength obtained by Eq. (3) using different inclusion sizes with experimental data at different stress ratios. (a) R=-1, (b) R=-0.5, (c) R=0.1, and (d) R=0.3.

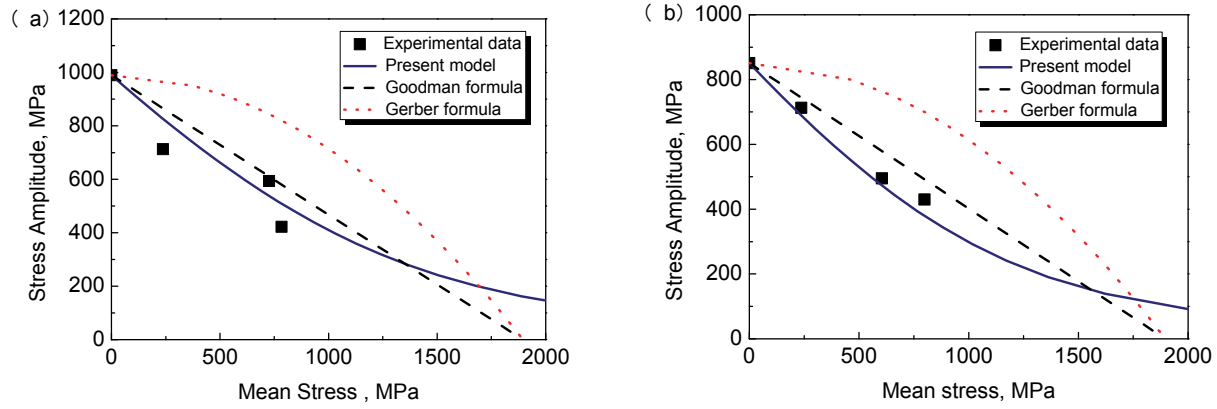

Figure 10: Comparison of predicted fatigue strength by present model, Goodman formula and Gerber formula with experimental data. (a) Fatigue strength at fatigue life of 10^8, and (b) Fatigue strength at fatigue life of 10^9.

Fig. 10 shows the comparison of the predicted fatigue strength by the present model, Goodman formula and Gerber formula with experimental data. The parameter α in the present model in Fig. 10 is taken as -0.713. It is seen that the present model is better in agreement with the experimental data in VHCF regime. The predicted fatigue strength by Goodman formula is larger than the experimental data, while the predicted value by Gerber formula has very big error with the experimental data.

Conclusions

The effects of stress ratio and inclusion size on the fatigue property of a high-strength steel in VHCF regime were investigated. The following conclusions are drawn.

(1) Fatigue strength decreases with the increase of stress ratio. The tendency of the S-N curves from low-cycle fatigue to VHCF fatigue is similar for different stress ratios. Fatigue crack initiates from the surface of specimen in low-cycle fatigue regime and initiates mostly from the inclusion in the interior of specimen for high-cycle and VHCF regimes, which is irrespective of stress ratio.

(2) The morphology of FGA is clear for the stress ratios of -1 and -0.5, and becomes obscure for the stress ratios of 0.1 and 0.3. The observation of microstructure below the FGA at R=-1 by TEM verifies the existence of fine granular area. Further, the absence of fine grains at R=0.3 indicated that FGA was generated by the numerous cyclic pressing between crack surfaces.

(3) The effect of stress ratio and inclusion size on fatigue strength is in good agreement with the formula of $\sigma_a \propto a_0^m[(1-R)/2]^\alpha$, where m is -1/6 and α is -0.713. The comparison with Goodman formula and Gerber formula indicates that the present model is better to correlate stress ratio and fatigue strength for VHCF regime.

Acknowledgements

The research of this paper was supported by the National Basic Research Program of China (No: 2012CB937500) and by the National Natural Science Foundation of China (Nos: 11172304 and 11202210).

References

[1] Zhao, A., Xie, J., Sun, C., Lei, Z., Hong, Y., Effects of strength level and loading frequency on very-high-cycle fatigue behavior for a bearing steel, Int. J. Fatigue, 38 (2012) 46-56. DOI: 10.1016/j.ijfatigue.2011.11.014

[2] Oguma, H., Nakamura, T., The effect of microstructure on very high cycle fatigue properties in Ti–6Al–4V, Scripta Mater., 63 (2010) 32-34. DOI: 10.1016/j.scriptamat.2010.02.043

[3] Naito, T., Ueda, H., Kikuchi, M., Fatigue behavior of craburized steel with internal oxides and nonmartensitic microstructure neear the surface, Metall. Mater. Trans. A, 15 (1984) 1431-1436. DOI: 10.1007/bf02648572

[4] Kikuchi, M., Ueda, H., Naito, T., Fatigue behavior of carburized steel with internal oxides near the surface, Metall. Mater. Trans. A, 18 (1987) 156-158. DOI: 10.1007/bf02646234

[5] Sakai, T., Sato, Y., Oguma, N., Characteristic S–N properties of high-carbon–chromium-bearing steel under axial loading in long-life fatigue, Fatigue Fract. Eng. Mater. Struct., 25 (2002) 765–773. DOI: 10.1046/j.1460-2695.2002.00574.x

[6] Zhao, A., Xie, J., Sun, C., Lei, Z., Hong, Y., Prediction of threshold value for FGA formation, Mater. Sci. Eng. A, 528 (2011) 6872–6877. DOI: 10.1016/j.msea.2011.05.070

[7] Nguyen, H.Q., Gallimard, L., Bathias, C., Numerical simulation of the coupling between thermal dissipation and fish-eye crack growth in very high cycle fatigue regime, Fatigue Fract. Eng. Mater. Struct., 36 (2013) 450–461. DOI: 10.1111/ffe.12016

[8] Sakai, T,. Lian, B., Takeda, M., Shiozawa, K., Oguma, N., Ochi, Y., Nakajima, M., Nakamura, T., Statistical duplex S–N characteristics of high carbon chromium bearing steel in rotating bending in very high cycle regime, Int. J. Fatigue, 32 (2010) 497-504. DOI: 10.1016/j.ijfatigue.2009.08.001

[9] Murakami, Y., Nomoto, T., Ueda, T., Murakami, Y., On the mechanism of fatigue failure in the superlong life regime (N > 10^7 cycles) Part I: influence of hydrogen trapped by inclusions, Fatigue Fract. Eng. Mater. Struct., 23 (2000) 893-

902. DOI: 10.1046/j.1460-2695.2000.00343.x
[10] Shiozawa, K., Morii, Y., Nishino, S., Lu, L., Subsurface crack initiation and propagation mechanism in high-strength steel in a very high cycle fatigue regime, Int. J. Fatigue, 28 (2006) 1521-1532. DOI: 10.1016/j.ijfatigue.2005.08.015
[11] Stanzl-Tschegg, S., Very high cycle fatigue measuring techniques, Int. J. Fatigue, 60 (2014) 2-17. DOI: 10.1016/j.ijfatigue.2012.11.016
[12] Paolino, D. S., Tridello, A., Chiandussi, G., Rossetto, M., On specimen design for size effect evaluation in ultrasonic gigacycle fatigue testing, Fatigue Fract. Eng. Mater. Struct., 37 (2014) 570–579. DOI: 10.1111/ffe.12149
[13] Kovacs, S., Beck, T., Singheiser, L., Influence of mean stresses on fatigue life and damage of a turbine blade steel in the VHCF-regime, Int. J. Fatigue, 49 (2013) 90-99. DOI: 10.1016/j.ijfatigue.2012.12.012
[14] Sander, M., Müller, T., Lebahn, J., Influence of mean stress and variable amplitude loading on the fatigue behaviour of a high-strength steel in VHCF regime, Int. J. Fatigue, 62 (2014) 10-20. DOI: 10.1016/j.ijfatigue.2013.04.015
[15] Shiozawa, K., Hasegawa, T., Kashiwagi, Y., Lu, L., Very high cycle fatigue properties of bearing steel under axial loading condition. Int. J. Fatigue, 31 (2009) 880-888. DOI: 10.1016/j.ijfatigue.2008.11.001
[16] Sakai, T., Sato, Y., Nagano, Y., Takeda, M., Oguma, N., Effect of stress ratio on long life fatigue behavior of high carbon chromium bearing steel under axial loading, Int. J. Fatigue, 28 (2006) 1547-1554. DOI: 10.1016/j.ijfatigue.2005.04.018
[17] Murakami, Y., Nomoto, T., Ueda, T., Factors influencing the mechanism of superlong fatigue failure in steels, Fatigue Fract. Eng. Mater. Struct., 22 (1999) 581-590. DOI: 10.1046/j.1460-2695.1999.00187.x
[18] Murakami, Y., Endo, M., Effects of Defects, inclusions and inhomogeneities on fatigue-strength, Int. J. Fatigue, 16 (1994) 163-182. DOI: 10.1016/0142-1123(94)90001-9
[19] Sun, C., Lei, Z., Hong, Y., Effects of stress ratio on crack growth rate and fatigue strength for high cycle and very-high-cycle fatigue of metallic materials, Mech. Mater.., 69 (2014) 227-36. DOI: 10.1016/j.mechmat.2013.10.007
[20] Sun, C., Lei, Z., Xie, J., Hong, Y., Effects of inclusion size and stress ratio on fatigue strength for high-strength steels with fish-eye mode failure, Int. J. Fatigue, 48 (2013) 19-27. DOI: 10.1016/j.ijfatigue.2012.12.004
[21] Hong, Y., Liu, X., Lei, Z., Sun C., Numerous cyclic pressing mechanism of crack initiation for very-high-cycle fatigue of metallic materials, submitted.